Title

Heteroaggregation of engineered nanoparticles and kaolin clays in aqueous environments

Authors

Wang, Hongtao
Dong, Ya-nan
Zhu, Miao
et al.

Publication Date

2015-09-01

DOI

10.1016/j.watres.2015.05.023

Peer reviewed

Water Research 80 (2015) 130–138

Contents lists available at ScienceDirect

Water Research

journal homepage: www.elsevier.com/locate/watres

Heteroaggregation of engineered nanoparticles and kaolin clays in aqueous environments

Hongtao Wang [a, *], Ya-nan Dong [a], Miao Zhu [a], Xiang Li [a], Arturo A. Keller [b], Tao Wang [a], Fengting Li [a]

[a] State Key Laboratory of Pollution Control and Resource Reuse, Key Laboratory of Yangtze River Water Environment, Ministry of Education, College of Environmental Science and Engineering, Tongji University, Shanghai, 200092, China
[b] Bren School of Environmental Science and Management, University of California, Santa Barbara, CA, 93106, United States

ARTICLE INFO

Article history:
Received 12 January 2015
Received in revised form
8 May 2015
Accepted 12 May 2015
Available online 14 May 2015

Keywords:
Nanoparticles
Humic acid
Kaolin
Critical coagulation concentration
Aggregation

ABSTRACT

The increasing and wide use of nanoparticles (NPs), including TiO_2 and Ag NPs, have raised concerns due to their potential toxicity and environmental impacts. Kaolin is a very common mineral in aquatic systems, and there is a very high probability that nanoparticles (NPs) will interact with these clay minerals. We studied the effect of kaolin particles on the aggregation of NPs under different conditions, including the role of pH, ionic strength (IS), and humic acid (HA). We show that kaolin reduces the energy barrier and the Critical Coagulation Concentration (CCC) at pH 4. At pH 8, even though the energy barrier of the system without kaolin increases, kaolin promotes NP aggregation via heteroaggregation. When IS is equal to or greater than the CCC, on the one hand HA promotes aggregation of TiO_2 NPs, but on the other hand HA decreases the rate of Ag NP aggregation because the existence of a surface coating may limit the adsorption of HA on these Ag NPs. In addition, the presence of HA increases the energy barrier and the CCC of the binary system (kaolin + NPs). Thus, the complex interactions of clay, NPs, IS, pH, and HA concentration determine the colloidal stability of the NPs. We find that kaolin is a potential coagulant for removal of NPs that behave like Ag and TiO_2.

1. Introduction

The rapid growth of nanotechnology applications in consumer and industrial products in the past few years has increased the release of nanoparticles (NPs) to the environment (Keller et al., 2013; Theron et al., 2008). TiO_2 NPs are used in many products, including paints, pigments and personal care products, and Ag NPs are used in many consumer products that can result in transfer to the aqueous environment via wastewater treatment plants (WWTPs) (Keller et al., 2013; Lazareva and Keller, 2014). A recent study estimated that 10–30%, 3–17% and 4–19% NPs are discarded into water bodies in Asia, Europe and North America respectively and predicted release concentrations of engineered nanomaterials in WWTP effluent of 5–20 μg/L TiO_2 NPs and 0.05–0.2 μg/L Ag NPs (Keller and Lazareva, 2013). Westerhoff et al. found effluent concentrations of TiO_2 NPs in WWTPs were still 25 μg/L titanium, even though the WWTPs removed more than 96% of the influent titanium (Westerhoff et al., 2011). The increasing understanding of the toxicity (Chen et al., 2006; Colvin, 2003; De Jong et al., 2013; Ghosh et al., 2013; Keller et al., 2010; Olmedo et al., 2005; Song et al., 2013; Trouiller et al., 2009; Zhang et al., 2007) of these NPs indicates that their potential risk can't be ignored, therefore, their fate, transport and removal need to be better understood.

Kaolin is an abundant clay material, found in many natural waters, and with high potential for wastewater treatment through adsorption due to its large surface area and pore volume (Ma and Wang, 2006; Ma et al., 2007). It should be noted that kaolinite is the clay mineral that characterizes/makes up most kaolin (Ross and Kerr, 1930). In this paper, we use kaolin to denote the clay material. Kaolin is divided into two kinds: a well-crystallized form (Zettlitz, with a Critical Coagulation Concentration (CCC)≈3 mM NaCl at pH = 4, and CCC ≈ 100 mM NaCl at pH = 8) and a poorly-crystallized form (KGa-2, unstable at pH = 4, CCC ≈ 85 ± 5 mM NaCl at pH = 9.5). The cation exchange capacity (CEC) of well-crystallized kaolin (≈9 meq/100 g) has almost three times greater permanent charge than poorly-crystallized kaolin (3.3 meq/100 g) (Tombacz and Szekeres, 2006; Van Olphen and Fripiat, 1979).

* Corresponding author.
E-mail address: hongtao@tongji.edu.cn (H. Wang).

http://dx.doi.org/10.1016/j.watres.2015.05.023
0043-1354/

Kaolin has one Al–O face and one Si–O face. The Si–O face has a negative charge because of lattice ion replacement. In addition, kaolin has an edge which is around 10–120 nm (Brady et al., 1996; Wan and Tokunaga, 2002). Compared with the defective (poorly-crystallized) crystal face, the surface charge density of the pristine (original or untreated) crystal face is higher, and the electric double layer (EDL) is thicker (Wan and Tokunaga, 2002). At low IS (10 mmol/L NaCl) and pH < $pH_{pzc,\ edge}$ (edge point of zero charge, pzc), the thickness of the EDL (Debye length ≈3 nm at 10 mmol/L) is larger than that of the thin lamella, and the dominant EDL extending from the face spills over the edge, screening the positive charge of the edge. This explains why at pH 4 poorly-crystallized kaolin is unstable at any IS, while well-crystallized kaolin is stable at low IS (Tombacz and Szekeres, 2004).

Humic substances represent an active and important fraction of natural organic matter (NOM) and they play important roles in the fate and transport of pollutants in the aqueous phase (Aiken, 1985; Buffle et al., 1998; Wang et al., 2011, 2010; Zheng et al., 2008). For example, humic acid (HA) affects the stability of NPs through electric forces, steric hindrances, and the bridging effect (Zhu et al., 2014). HA also reduces the removal of TiO_2 NPs by coagulation (Wang et al., 2014, 2013). The presence of NOM, and in particular HA, has been shown to contribute to the instability of Ag NPs at high ionic strength in divalent metallic cation solutions, most likely due to intermolecular bridging with the organic matter (Akaighe et al., 2012).

In recent years, the transport of NPs in natural systems, especially the interaction between NPs and clay particles has attracted much attention (Afrooz et al., 2013; Huynh et al., 2012; Labille et al., 2015; Praetorius et al., 2014; Zhao et al., 2015). For example, Liang et al. (2013) studied the transport of Ag NPs and their interaction with clay particles in soils, and Cai et al. (2014) discussed the combined effects of IS and clay particles on the transport of TiO_2 NPs in quartz sand. These studies mainly focused on the effect of pH, IS and clay particles, but some studies show that NOM also plays an important role in the stability of NPs, such as stabilization due to the adsorption of NOM, or enhanced coagulation due to the bridging effect of NOM (Chen and Elimelech, 2007a; Mohd Omar et al., 2014; Zhu et al., 2014). Furthermore, montmorillonite was shown to destabilize engineered NPs due to heteroaggregation (Zhou et al., 2012). Since kaolin is a widely available clay, its role in heteroaggregation should be studied.

The goal of this study was to evaluate the effects of kaolin particles and of NOM on the heteroaggregation of engineered nanoparticles in aqueous environments. In this study, the stability of NPs, NPs-kaolin, NPs-HA, and NPs-kaolin-HA systems were evaluated under different pH and IS conditions. CCC and aggregation rate were used to determine the stability of the NPs via DLS measurements.

2. Methods and materials

2.1. TiO_2 nanoparticles

TiO_2 Nanoparticles (rutile) were purchased from Sigma–Aldrich Trading Co., Ltd. (Shanghai), product number 53680-10G. According to the manufacturer, the transmission electron microscopy (TEM) size of the nanoparticles is 10 nm × 40 nm (diameter × length); their specific surface area is around 130–190 m^2/g; their purity is around 99.5%. We used SEM and TEM images to characterize the size and shape of these nanoparticles (Fig. S1), and measured their pH_{pzc} with a Malvern Zetasizer (Fig. S2, pH_{pzc} ~6). An appropriate amount of TiO_2 NPs was placed in Millipore water and sonicated for 20 min (Qi et al., 2013) to achieve a 1 g/L TiO_2 NP stock suspension. Fresh stock suspensions were prepared daily.

2.2. Ag nanoparticles

A nanosilver dispersion (25 ml) was purchased from Sigma–Aldrich Trading Co., Ltd. (Shanghai), product number 730807. The diameter of these nanoparticles is around 40 nm (Fig. S4). These particles contain sodium citrate as stabilizer, thus they carry a negative charge at pH 4 and 8. The concentration of the suspension is 20 mg/L. For the experiments the suspension was diluted to 2 mg/L; this was the minimum concentration at which nanoparticles could be detected reliably via Dynamic Light Scattering (DLS).

2.3. Kaolin

Kaolin (K7375) was purchased from Sigma–Aldrich Trading Co., Ltd. (Shanghai). To produce an aqueous slurry, 200 g kaolin and 0.3 g Na_2CO_3 were added to 100 ml Millipore water. To remove and replace the Ca^{2+} contained in the kaolin with Na^+ so as to meet the requirement of the DLVO calculation (Zhou et al., 2012), the slurry was heated in a water bath at about 80 °C for 2 days then diluted using Millipore water to achieve a nominal concentration of 4 g clay in a 100 ml suspension, following Tombacz and Szekeres (2006). To obtain a fraction smaller than 2 μm, the larger particles were allowed to settle and then the supernatant was separated by decanting. Excess carbonate was eliminated by HCl addition. To obtain monocationic Na-kaolin, the suspension was treated with 1 M NaCl. After centrifuging the suspension at 3600 revolutions per minute (RPM), the supernatant was discarded and replaced with fresh solution (0.01 M NaCl). The procedure was repeated three times. The IS of the suspension was progressively lowered, first by washing with Millipore water and then by dialysis against 0.01 M NaCl. An MWCO 12–14K membrane (Spectrumlabs, USA) was used to dialyze the suspension. The progress of dialysis was controlled by measuring the conductivities of inner and outer phases daily. This procedure was repeated five times. The Na-kaolin suspension (≈200 g/L) in the dialysis tubes reached an equilibrium state within 4 days (Tombacz and Szekeres, 2006). The stock Na-kaolin suspensions were stored at 4–5 °C. Before DLS measurements, the stock suspension was diluted using Millipore water to 3 g/L and then centrifuged at 4000 RPM for 3 min. DLS measurements were conducted on the supernatant. The Z-average size of the kaolin particles was around 263 nm, and the TEM images show that the size range of Kaolin can be as great as 500 nm (Fig. S3). As Fig. S5 shows, the kaolin crystal consists of alternating layers of silica tetrahedra and alumina octrahedra and the unit cell of the kaolin lattice has the composition $[Si_2Al_2O_5(OH)_4]$. Each kaolin particle consists of a stack of about 50 sheets of twin-layers, held together with hydrogen bonds. The particles are plate-like and the aspect ratio (particle diameter: particle thickness) is about 5–15, depending on the mechanical treatment of kaolin (Nandi et al., 2009; Solomon and Hawthorne, 1983).

2.4. Humic acid preparation

Humic acid (53680-10G) was purchased from Sigma–Aldrich (Shanghai) Trading Co., Ltd. The HA stock solution was prepared by dissolving a certain amount of HA powder into deionized water, and adjusting the pH to 11 by adding 0.1 M NaOH, then stirring the solution at 600 RPM for 24 h to improve the solution stability. A 0.25 μm filter membrane was used to remove the insoluble fraction. The stock solution was preserved under 5 °C. The Total Organic Carbon (TOC) of the HA stock solution was measured using a

Shimadzu TOC-V, and the stock solution was diluted to 10.5 mg/L as TOC.

2.5. Buffer solutions

To control pH, 1 mM sodium acetate-acetic acid buffer (pH = 4), 1 mM acetic acid-sodium acetate buffer (pH = 5 and 6), 1 mM disodium hydrogen phosphate-sodium dihydrogen phosphate buffer (pH = 7), and 1 mM boric acid-borax buffer (pH = 8) were used.

2.6. Potentiometric acid-base titration (kaolin)

Lower valence cations (such as Fe^{2+}, Mg^{2+}) frequently substitute Si^{4+} or Al^{3+} at the tetrahedra/octahedra sites of kaolin, resulting in net negative charges on the Si–O face. At the edge and Al–O face of the kaolin lamella where the extended Si–Al structure breaks, amphoteric Si–OH and Al–OH groups and thus variable charges develop (Van Olphen, 1963). At a pH below $pH_{pzc,\ edge}$, the Si–O face carries negative charges while the edge and Al–O face carry positive charges; at pH higher than the $pH_{pzc,\ edge}$, the entire platelet is negatively charged with a non-uniform charge density (Tombacz and Szekeres, 2006).

The $pH_{pzc,\ edge}$ of kaolin can be measured through a potentiometric acid-base titration method (Tombacz and Szekeres, 2006). The pH-dependent surface charge of kaolin was determined by potentiometric acid–base titration under a CO_2-free atmosphere using NaCl to maintain a constant IS (0.1 mM). Before titration the suspensions containing ≈1 g/L kaolin were stirred and bubbled with purified nitrogen for an hour. A pH/ion Meter (781, Metrohm) was used to measure the equilibrium titration at 25 °C. The titration was performed by adding NaOH to increase pH from 3 to 9 (Tombacz and Szekeres, 2006). The net proton surface excess amount ($\Delta n^{\sigma}_{H/OH}$, mol/g) is defined as a difference of H^+ and OH^- surface excess amounts (n^{σ}_{H+} and n^{σ}_{OH-}, respectively) related to unit mass of solid, $\Delta n^{\sigma}_{H/OH} = n^{\sigma}_{H+} - n^{\sigma}_{OH-}$. The surface excess amount of any solute, like H^+ and OH^- here, can be determined directly from the initial and equilibrium concentration of solute for adsorption from dilute solution. The $n\sigma_{H+}$ and n^{σ}_{OH-} were calculated at each point of titration from the electrode output using the actual activity coefficient from the slope of H^+/OH^- activity vs. concentration straight lines for background electrolyte titration (Everett, 1986). As shown in Fig. S6, the points were calculated from the data of equilibrium titration cycles to test the reversibility of acid–base processes: first a backward titration from pH = 5.6 to 3.5 (black squares) with 0.1 M HCl solution, then a forward cycle from pH = 3.5 to 9.5 (red circle) with 0.1 M NaOH solution, finally a backward titration from pH = 9.5 to 3.5 (blue triangles) again. The $pH_{pzc,\ edge}$ of kaolin is 5–6 (Fig. S6).

2.7. Coagulation kinetics

Coagulation kinetics for the various particles were measured by collecting time-resolved hydrodynamic size data of the particle suspension using DLS (Zetasizer nano, Malvern, UK). NaCl (ranging from 0 to 1.5 M in 0.1 M increments) was used to provide IS. DLS measurements were started immediately after mixing NaCl solution, buffer solution and particles suspension. Each measurement lasted for 30 s. The instrument employs a 633 nm laser with a detection angle of 90°. Data collection was ended after 1 h or until the hydrodynamic size doubled, depending on whichever criteria was met first (Zhou et al., 2012). The ratio of the coagulation rate in the presence of an energy barrier to that in the absence of an energy barrier is defined as the attachment efficiency (α), which is calculated as follows (Elimelech et al., 1995):

$$\alpha = \frac{1}{W} = \frac{\left(\frac{d_{r_H}}{d_t}\right)_{t\to 0}}{\left(\frac{d_{r_H}}{d_t}\right)_{t\to 0,\,fast}}$$

Here r_H is the hydrodynamic radius; $(d_{rH}/d_t)_{t\to 0,fast}$ is the average of the highest, relatively constant rates observed experimentally for a given set of conditions. The CCC is the IS at which α reaches a constant value of unity (Zhou et al., 2012). In this research, k_{fast}, which is equal to $(d_{rH}/d_t)_{t\to 0,fast}$, was used to reflect the particles' maximum aggregation rate at high IS. As IS increases, the attachment efficiency increases because of screening of the NPs surface charge (reaction-limited cluster aggregation regime, RLCA). When the NaCl concentration reaches and surpasses the CCC, the surface charge of nanoparticles is completely screened, and eliminates the energy barrier (diffusion-limited cluster aggregation regime, DLCA). CCC can be determined by the intersection of RLCA and DLCA (Chen and Elimelech, 2007b).

2.8. DLVO calculation

The energy barrier between NPs and clay under different IS and pH in the presence and absence of humic acid was calculated by DLVO theory (see supporting information). Sphere–sphere and sphere-plate models were used to calculate energy barrier for NPs–NPs and NPs-kaolin system. The current experimental conditions justify the applicability of the DLVO theory (Zhou et al., 2012): (1) the particle concentrations are relatively dilute, (2) kaolin is in its sodium form, and (3) the particle charges are relatively low (Fig. S2, Fig. S7). To further investigate the effect of humic acid, $\gamma^{LW}_{HA} = 25.77\ mJ/m^2$ (Hu et al., 2010) at TOC = 1 mg/L was used to calculate the energy barrier under the effect of humic acid. γ^{LW}_{X} is the Lifshitz-vander Waals component of the surface free energy of the particle (x = p) or the water/humic acid solution (x = w). $\gamma^{LW}_{water} = 21.8\ mJ/m^2$ (Hu et al., 2010).

3. Results

3.1. TiO_2 NP-kaolin binary system

Fig. 1 shows the stability of TiO_2 NPs in the absence and presence of kaolin at pH 4 and 8. The stability of TiO_2 NP suspension at pH 8 (CCC ≈ 60 mM) is very similar to that at pH 4 (CCC ≈ 50 mM). Kaolin is stable at pH 8 (CCC ≈ 100 mM) while it aggregates rapidly at pH 4 even at very low IS. At pH 4, the TiO_2 NPs-kaolin binary system is unstable, and the attachment efficiency is 1 even at very low IS (<1 mM). To further determine the interaction of TiO_2 NPs and kaolin, the supernatant turbidity was measured. Table S1 shows that kaolin destabilizes TiO_2 NPs at low IS and pH 4. Table S2 shows that kaolin increases the aggregation rate of TiO_2 NPs at low IS and pH 4. Based on the structure of kaolin, we propose the following mechanism: due to electrostatic attraction between the Al–O face/edge (+) and Si–O face (−), kaolin rapidly aggregates even in the absence of IS at pH 4; under these conditions TiO_2 NPs (+) are attracted to the Si–O face. Therefore, kaolin promotes the removal of TiO_2 NPs via heteroaggregation, followed by settling of the kaolin aggregates. Compared with pH 4, the system is relatively stable at pH 8, where TiO_2 NPs, kaolin edges, Al–O faces and Si–O faces all carry negative charges, and electrical repulsion increases system stability. However, as IS increases up to the CCC, the aggregation rate of the TiO_2 NPs in the presence of kaolin increases remarkably compared with that in the absence of kaolin (Table S2). Generally the stability of the binary TiO_2-kaolin system decreases slowly from pH 8 to 5, but then becomes very unstable at pH 4

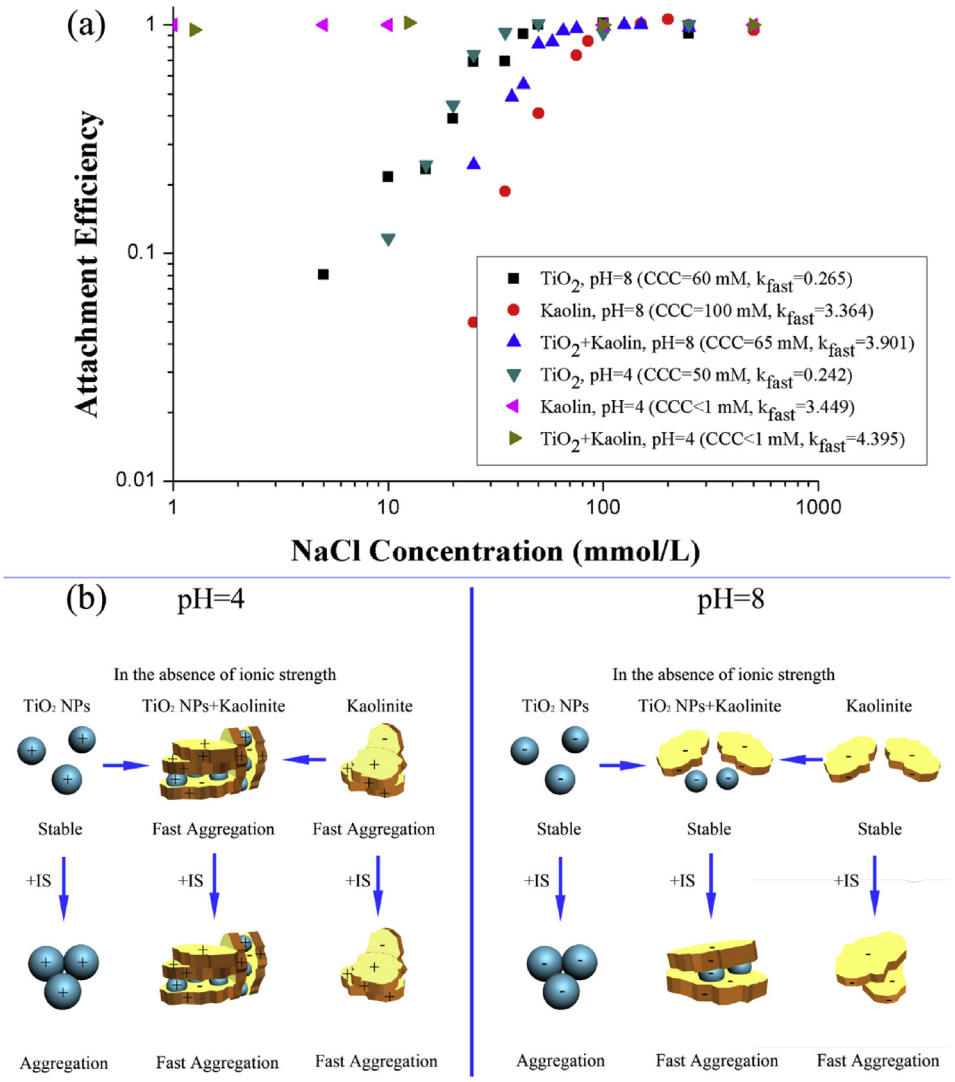

Fig. 1. (a) Attachment efficiency of kaolin, TiO_2 NPs, and kaolin + TiO_2 NPs binary system ([kaolin] = 50 mg/L, [TiO_2] = 10 mg/L); (b) Proposed mechanism of kaolin and TiO_2 NPs interaction.

(Table S4). Even near the pH_{pzc} of TiO_2 (~pH 6) the CCC of the binary system is around 50 mM.

3.2. Ag NP-kaolin binary system

Fig. 2 shows that the CCC of Ag NPs is not very pH sensitive, 50 mM at pH 4 and 40 mM at pH 8. The Ag NPs used in this study carry a negative charge at a pH range from 4 to 8 (Fig. S7), due to their citrate coating (Thio et al., 2012). Unlike the TiO_2 NP-kaolin system, kaolin has no distinct destabilization effect on Ag NPs at pH = 4 and low IS (IS = 0 mM or IS = 10 mM, $\alpha \approx 0$ for the Ag + kaolin binary system, hydrodynamic data shown in Fig. S10). In addition, the presence of kaolin increases the CCC at pH 8, because kaolin increases electrical repulsion and the energy barrier (Fig. S9). Since the size of the TiO_2 NPs (diameter × length of 10 nm × 40 nm) is close to the Ag NPs (diameter = 40 nm), the difference in behavior between TiO_2 NP-kaolin system and Ag NP-kaolin system is likely to be caused by the surface potential. We propose that the same mechanism described above for TiO_2 is also valid for Ag NPs, but the differences in zeta potential at different pH result in a different behavior. At pH 4, Ag NPs (−) might be absorbed on the Al—O face (+) and edge (+). Therefore, the presence of Ag NPs is likely to screen the surface positive potential on the Al—O face and edges, minimizing the interaction between the Al—O face (+) in one particle with the Si—O face (−) of another, as well as the edges (+) and Si—O faces (−), thus resulting in a more stable Ag NP-kaolin system. Though the Ag NP-kaolin system is stable at pH 4, the presence of kaolin reduces the CCC. However, CCC increases sharply from 40 mM at pH 4–200 mM at pH 5, and then more slowly to 300 mM at pH 8 (Table S4).

3.3. TiO_2 NP-HA binary system

Fig. 3 shows that the CCCs of the TiO_2 NP-HA binary system are 250 mM at pH 4 and 500 mM at pH 8, which are much higher than without HA; HA makes the system more stable. However, Table S2 indicates that the presence of HA promotes fast TiO_2 aggregation when IS approaches CCC. The adsorption of HA on TiO_2 NPs was reported in our recent work (Zhu et al., 2014). The difference in interactions explains the difference in CCC at pH 4 and pH 8. At pH 4, HA is negative and the surface charge of TiO_2 NPs is positive, so adsorption occurs through electrostatic attraction at pH < pH_{pzc} (TiO_2 NPs); at pH 8, both the surface charge on the TiO_2 NPs and the charge of HA are negative, so electrostatic repulsion limits the

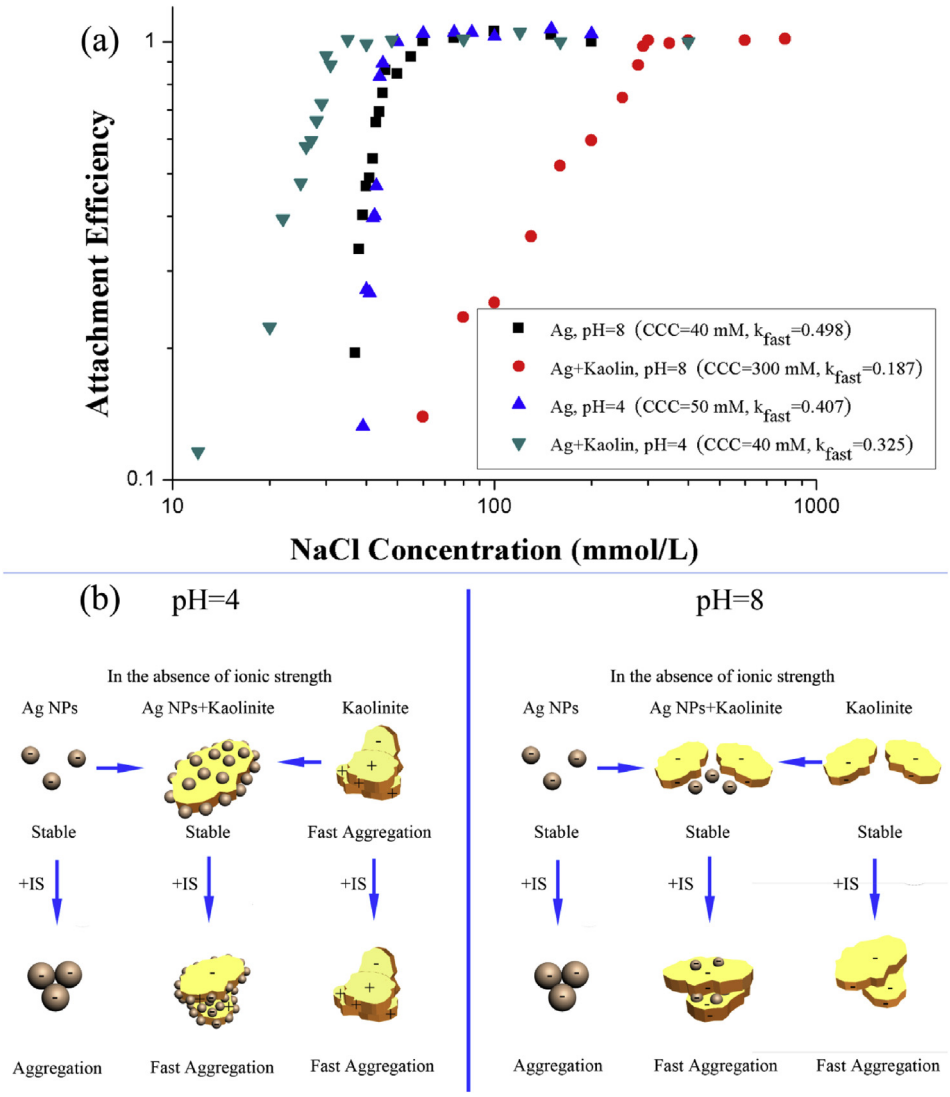

Fig. 2. (a) Attachment efficiency of Ag NPs and Ag NPs + kaolin binary system ([kaolin] = 50 mg/L, [Ag NPs] = 5 mg/L); (b) Proposed mechanism of Ag NPs and kaolin interaction.

adsorption of HA to the TiO_2 NPs, and HA is absorbed on the TiO_2 NPs via the Ti–O bond (Zhu et al., 2014).

3.4. Ag NP-HA binary system

Fig. 4 and Table 1 show that the CCCs of the Ag NP-HA binary system are 600 mM at pH 4 and 100 mM at pH 8. Table S2 indicates that the presence of HA reduces the aggregation rate of Ag NPs when IS reaches CCC. Ag NPs behave differently from TiO_2 NPs in the presence of HA. Unlike TiO_2 NPs, the zeta potential of Ag NPs barely changes at pH 4 and pH 8 in the presence of HA under different NaCl concentrations (Fig. S7). This may be caused by the citrate coating, which limits the interaction between Ag NPs and HA. Our preliminary results also show that only less than 10% HA was adsorbed onto Ag NPs. Though HA does not adsorb onto the Ag NPs, it still reduces the aggregation rate and increases CCC.

3.5. TiO_2 NP-kaolin-HA ternary system

Fig. 5 and Table 1 show that the CCCs of the TiO_2 NP-kaolin-HA ternary system at pH 8 are 200, 333 and 700 mM when [HA] = 0.1, 1 and 10 mg/L, respectively. At pH 4 the system is unstable when [HA] = 0.1 mg/L, but the CCC increases to 100 mM at [HA] = 1 mg/L and CCC = 300 mM at [HA] = 10 mg/L Table S2 also indicates that although a high concentration of HA (10 mg/L) decreases the aggregation rate (without kaolin), the additional presence of kaolin increases the aggregation rate of the system. At pH 4 the adsorption of HA (−) on the TiO_2 NPs (+), and Al–O face (+) and edges (+) of kaolin reduces and inverses the surface charge. At pH 8, adsorbed HA increases steric hindrance and thus the CCC. This ternary system is stabilized at 1 mg/L HA from pH 4 to 8 (Table S4), with CCC increasing almost continuously with increasing pH.

3.6. Ag NP-kaolin-HA ternary system

Fig. 6 and Table 1 show that the CCCs of the Ag-kaolin-HA ternary system at pH 8 are 300, 500 and 800 mM, while at pH 4 the CCCs are 100, 300, 700 mM when [HA] = 0.1, 1 and 10 mg/L, respectively. For Ag NPs, though the adsorption of HA on their surface is very low (the zeta potential barely changes with the addition of 1 mg/L HA), HA still increases the system's CCC and reduces the aggregation rate. This ternary system is even more stable with 1 mg/L HA in the range of pH from 4 to 8 (Table S4).

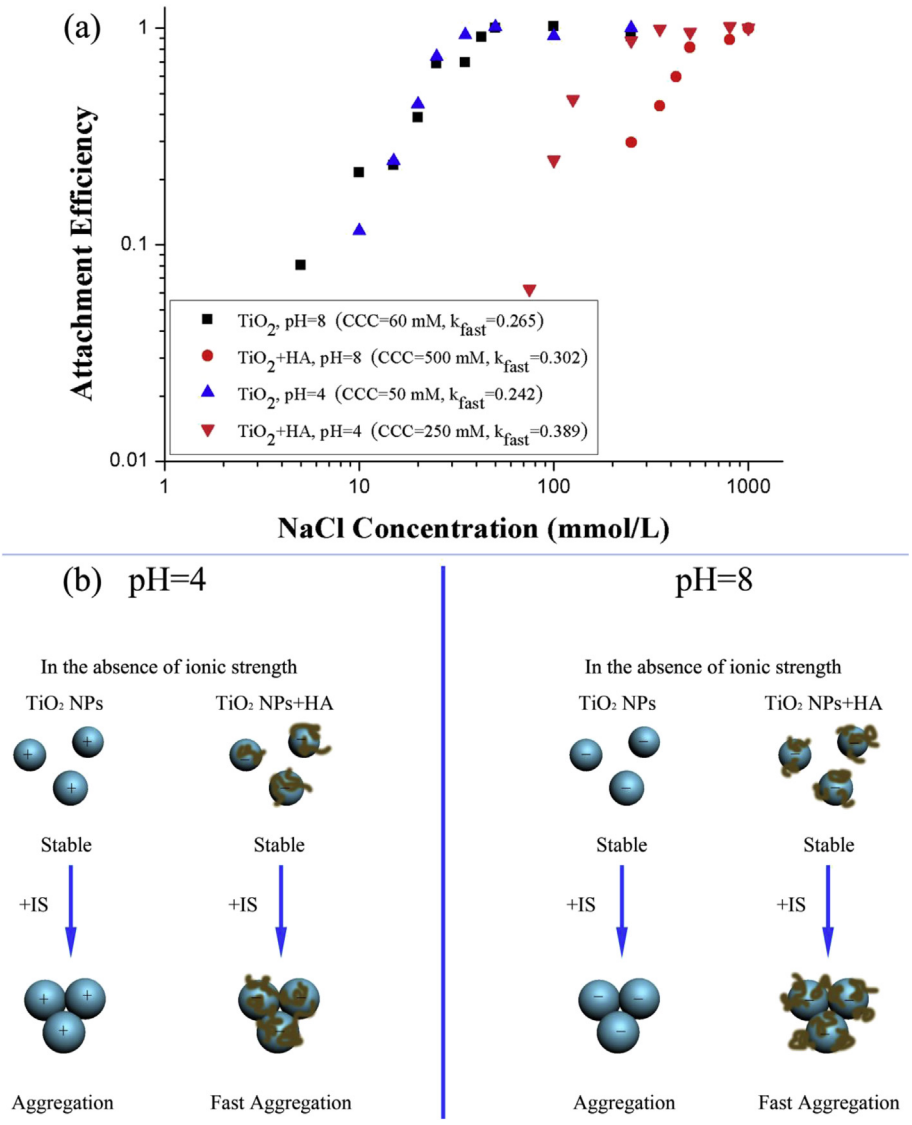

Fig. 3. (a) Attachment efficiency of TiO_2 NPs and TiO_2 NPs + HA binary system ([TiO_2] = 10 mg/L, [HA] = 1 mg/L); (b) Proposed mechanisms of TiO_2 NP aggregation as a function of IS at pH 8 and pH 4 in the presence and absence of HA.

4. Discussion

In the TiO_2 NP-kaolin binary system, the behavior of the kaolin-TiO_2 NP system differs from that observed using montmorillonite and TiO_2 NPs (Zhou et al., 2012). This is due to the structural differences between kaolin and montmorillonite. In the sheet-like structure of montmorillonite, two layers of Si-tetrahedra sandwich one layer of Al-octahedra. Each Si^{4+} is coordinated by four O^{2-} and each Al^{3+} is coordinated by six O^{2-}. The sheets are bonded together by Si^{4+} and Al^{3+} sharing O^{2-} ions (McBride, 1994). The $pH_{pzc,\ edge}$ of montmorillonite is around 6.5 by potentiometric titration (Tombacz and Szekeres, 2004). At pH 8, the CCC of the montmorillonite-TiO_2 NP binary system is around 50 mM (1:1 electrolyte) (Zhou et al., 2012). Both the TiO_2 NPs-montmorillonite and TiO_2 NPs-kaolin systems are stable at pH = 8 and up to their CCC. However, poorly-crystallized kaolin has a much more distinct destabilization effect on TiO_2 NPs at pH 4 and the system is completely unstable, compared with montmorillonite (CCC ≈ 10 mM) (Zhou et al., 2012). The edge thickness of kaolin (10–120 nm) is greater than that of montmorillonite (thickness ≈ 1 nm). For montmorillonite, since the thickness of the EDL is larger than that of the thin lamella, the dominant EDL extending from the particle faces spills over the edge at low IS, and results in screening the positive edge charge when $pH < pH_{pzc,\ edge}$ (Tombacz and Szekeres, 2004). However, for kaolin the edge thickness is greater than the EDL thickness (Debye length ≈ 10 nm in 1 mmol/L) (Brady et al., 1996), thus the dominant EDL cannot screen the edge and Al–O face, leaving exposed the positively charged edge and Al–O face region of lamellae at $pH < pH_{pzc,\ edge}$. Therefore, the energy barriers of Al–O face (+) to Si–O face (−), edge (+) to Si–O face (−) and TiO_2 NPs (+) to Si–O face (−) disappear at $pH < pH_{pzc,\ edge}$.

In the Ag NP-kaolin binary system, with increasing IS, the EDLs of kaolin and Ag NPs are compressed, and particles begin to aggregate. Table S2 indicates that the presence of kaolin enhances the aggregation rate of Ag NPs when IS reaches CCC. The high aggregation rate of kaolin is the key to promoting the aggregation of Ag NPs via electrostatic attraction (only at pH 4) and heteroaggregation.

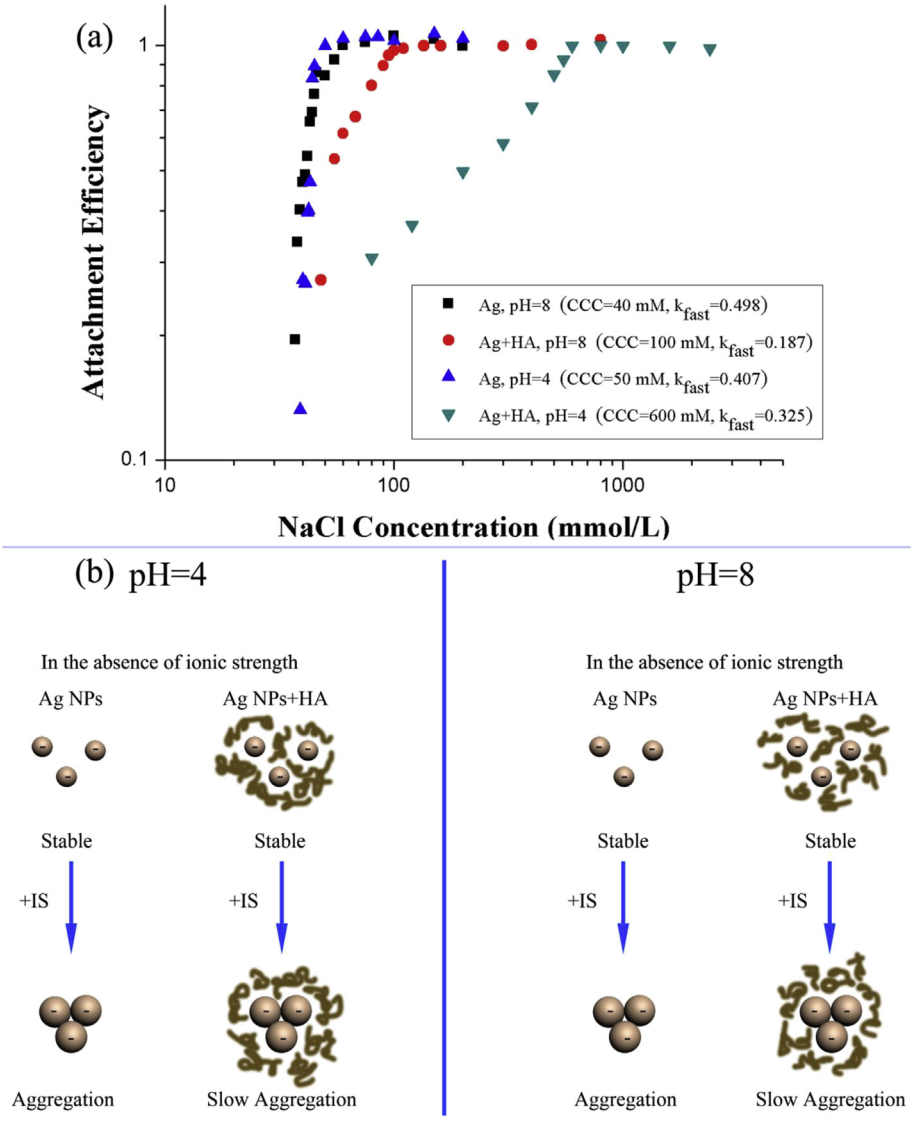

Fig. 4. (a) Attachment efficiency of Ag NPs and Ag NPs + HA binary system ([Ag] = 5 mg/L, [HA] = 1 mg/L); (b) Proposed mechanism of Ag NPs aggregation as a function of IS at pH 8 and pH 4 in the presence and absence of HA.

Table 1
CCC under different conditions at pH 4 and 8 ([TiO_2 NP] = 100 mg/L, [Ag NP] = 2 mg/L, [kaolin] = 50 mg/L, sodium chloride provides ionic strength. CCC in mmol/L, HA in mg/L).

pH	TiO_2	kaolin	Ag	TiO_2+kaolin	TiO_2+HA	kaolin + HA	Ag + kaolin	Ag + HA
8	60	100	40	65	500	250	300	100
4	50	<1	50	<1	250	75	40	600

pH	Ternary system (kaolin+)					
	TiO_2 + HA (0.1)	TiO_2 + HA (1)	TiO_2 + HA (10)	Ag + HA (0.1)	Ag + HA (1)	Ag + HA (10)
8	200	333	700	300	500	800
4	<1	100	300	100	300	700

Note: [HA] = 0.1, 1, 10 mg/L.

In the TiO_2 NP-HA binary system, the existence of HA on the surface of TiO_2 NPs causes steric hindrance to inhibit the TiO_2 NPs interacting with the ions. Therefore, CCC increases in the presence of HA. However, because of a bridging effect, the aggregation and sedimentation rates of TiO_2 NPs are promoted by HA when IS reaches CCC.

In the TiO_2 NP-kaolin-HA ternary system, HA enhances the energy barrier of the system to increase CCC and decrease the aggregation rate. However, the rapid aggregation rate of kaolin, the adsorption of HA, and the heteroaggregation of the TiO_2 NPs influence the behavior of this ternary system.

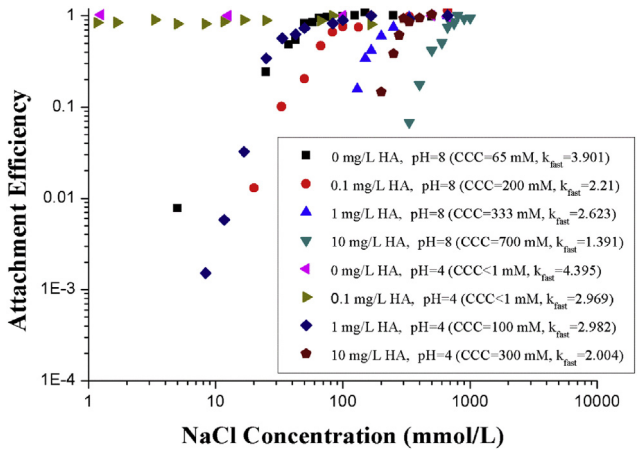

Fig. 5. Attachment efficiency of TiO_2-kaolin-HA ternary system ([kaolin] = 50 mg/L, [TiO_2] = 10 mg/L).

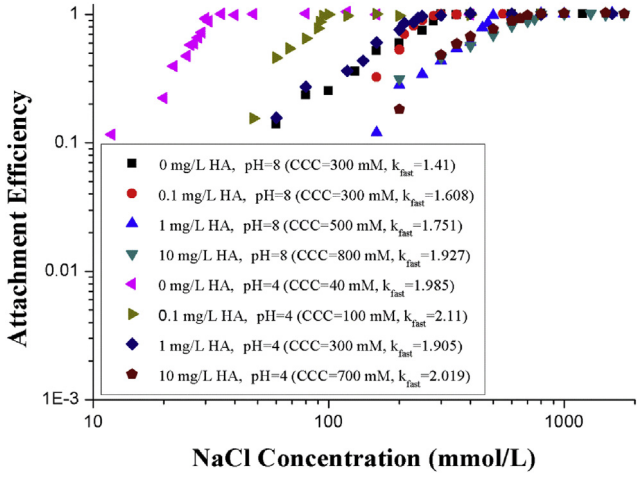

Fig. 6. Attachment efficiency of Ag-kaolin-HA ternary system ([kaolin] = 50 mg/L, [Ag] = 5 mg/L.

In the Ag NP-kaolin-HA ternary system, HA contributes with steric hindrance even if HA is not adsorbed significantly on the NPs. With the addition of HA, the adsorption of HA (−) on the Al–O face (+) and edge (+) reduces and inverses the surface charge of TiO_2 NPs, but there is no effect on the Ag NPs (−). Therefore, the energy barrier and CCC increase. Table S2 also shows that, compared to both NPs, the aggregation rate of the ternary system is more rapid once the CCC is reached.

Although it is reported Ag-NPs form Ag_2S in wastewater during treatment processes and it is less likely that metallic Ag-NPs will be present in surface waters (Kaegi et al., 2013), the use of Ag-NPs and kaolin helps to understand the fundamental mechanisms of heteroaggregation for these coated particles that do not transition from a positive to negative surface charge. These results can be used for input to environmental fate and transport models.

The results at pH 4 and 8 were presented since these conditions are further away from the IEP (~6.1) of TiO_2. However, we also measured the CCC and kinetics at pH 5, 6 and 7, to understand the transition as pH increases (Table S4). TiO_2 NPs are easily aggregated and precipitated at pH 6. The CCC of TiO_2 NPs is < 1 mM at pH 6. But the CCC of kaolin at pH 6 is much higher (70 mM), and the CCC of kaolin + TiO_2 NPs is 50 mM. For the Ag NPs, there is a transition from high stability at high pH to decreasing stability at low pH for the binary and ternary systems. In consideration that pH 4 and 8 can represent the mechanism of heteroaggregation between clay particles and NPs quite well, we only present the results of pH 4 and 8 in Table 1 and Table S2.

To determine the quantity of NPs destabilized by kaolin through heteroaggregation, we measured the residual NPs in the supernatant of the ternary system by ICP (Table S6). It was found that ~65% TiO_2 NPs were left in the supernatant after a short time for heteroaggregation (240 s at pH 4 and 360 s at pH 8), but only 21% TiO_2 NPs were found in the supernatant after 3 h of heteroaggregation. Similarly, only 14–17% of Ag NPs were detected in the supernatant after 3 h of heteroaggregation. This indicates that the TiO_2 and Ag NPs were involved in the heteroaggregation process.

5. Conclusions

The wide presence of clay particles and increasing discharge of NPs makes inevitable their interaction in natural aqueous systems. The complex interaction is determined by the combined effect of pH, IS, and HA. Because of the specific structure of kaolin, several interaction patterns occur under various conditions. The results show that kaolin particles can destabilize both positively and negatively charged NPs under various conditions in the subsurface and open water bodies. However, the presence of HA even at 1 mg/L can significantly modify the outcome, stabilizing the binary and ternary systems. There are significant differences between TiO_2 and citrate-coated Ag NPs, because their pH_{pzc} differ considerably. Although at pH 4 the systems are less stable, they can be quite stable at pH 8 under most conditions, even at very high IS (>200 mM). Since many natural waters have higher pH (7 and greater), this indicates that although the NPs will be adsorbed on kaolin, the presence of HA can result in significant mobility of the NPs in the water column, but attached to clays. Kaolin can be used as a low-cost and non-hazardous coagulant for NP removal, but the conditions need to be optimized to achieve effective sedimentation if there is HA present.

Acknowledgments

This work was supported in part by the National Natural Science Foundation of China Fund (No. 51108328). The research was also partially supported by 111 Project and the Fundamental Research Funds for the Central Universities (0400219276 and 0400219184) and State Key Laboratory of Pollution Control and Resource Reuse Foundation (No.PCRRY11011). This material is also partially supported by the U.S. National Science Foundation (NSF) and the U.S. Environmental Protection Agency (EPA) under Grant DBI-0830117. Any opinions, findings, and conclusions or recommendations expressed in this material are those of the authors and do not necessarily reflect the views of the NSF or EPA. This work has not been subjected to EPA review, and no official endorsement should be inferred. We also acknowledge the valuable comments from anonymous reviewers which help improve the quality of this paper.

Appendix A. Supplementary data

Supplementary data related to this article can be found at http://dx.doi.org/10.1016/j.watres.2015.05.023.

References

Afrooz, A.R.M.N., Khan, I.A., Hussain, S.M., Saleh, N.B., 2013. Mechanistic heteroaggregation of gold nanoparticles in a wide range of solution chemistry. Environ. Sci. Technol. 47 (4), 1853–1860.
Aiken, G., 1985. Humic Substances in Soil, Sediment, and Water: Geochemistry, Isolation, and Characterization. Wiley, New York.

Akaighe, N., Depner, S.W., Banerjee, S., Sharma, V.K., Sohn, M., 2012. The effects of monovalent and divalent cations on the stability of silver nanoparticles formed from direct reduction of silver ions by Suwannee river humic acid/natural organic matter. Sci. Total Environ. 441, 277–289.
Brady, P.V., Cygan, R.T., Nagy, K.L., 1996. Molecular controls on kaolinite surface charge. J. Colloid Interf. Sci. 183 (2), 356–364.
Buffle, J., Wilkinson, K.J., Stoll, S., Filella, M., Zhang, J.W., 1998. A generalized description of aquatic colloidal interactions: the three-colloidal component approach. Environ. Sci. Technol. 32 (19), 2887–2899.
Cai, L., Tong, M., Wang, X., Kim, H., 2014. Influence of Clay particles on the transport and retention of titanium dioxide nanoparticles in quartz Sand. Environ. Sci. Technol. 48 (13), 7323–7332.
Chen, H.W., Su, S.F., Chien, C.T., Lin, W.H., Yu, S.L., Chou, C.C., Chen, J.J.W., Yang, P.C., 2006. Titanium dioxide nanoparticles induce emphysema-like lung injury in mice. Faseb J. 20 (13), 2393.
Chen, K.L., Elimelech, M., 2007a. Influence of humic acid on the aggregation kinetics of fullerene (C60) nanoparticles in monovalent and divalent electrolyte solutions. J. Colloid Interf. Sci. 309 (1), 126–134.
Chen, K.L., Elimelech, M., 2007b. Influence of humic acid on the aggregation kinetics of fullerene (C60) nanoparticles in monovalent and divalent electrolyte solutions. J. Colloid Interf. Sci. 309 (1), 126–134.
Colvin, V.L., 2003. The potential environmental impact of engineered nanomaterials. Nat. Biotechnol. 21 (10), 1166–1170.
De Jong, W.H., Van Der Ven, L.T.M., Sleijffers, A., Park, M.V.D.Z., Jansen, E.H.J.M., Van Loveren, H., Vandebriel, R.J., 2013. Systemic and immunotoxicity of silver nanoparticles in an intravenous 28 days repeated dose toxicity study in rats. Biomaterials 34 (33), 8333–8343.
Elimelech, M.G., Jia, X., Williams, R., 1995. Particle Deposition and Aggregation: Measurement. Elsevier, New York.
Everett, D.H., 1986. Reporting data on adsorption from solution at the solid/solution interface. Pure Appl. Chem. 58, 967–984.
Ghosh, M., Chakraborty, A., Mukherjee, A., 2013. Cytotoxic, genotoxic and the hemolytic effect of titanium dioxide (TiO_2) nanoparticles on human erythrocyte and lymphocyte cells in vitro. J. Appl. Toxicol. 33 (10), 1097–1110.
Hu, J.-D., Zevi, Y., Kou, X.-M., Xiao, J., Wang, X.-J., Jin, Y., 2010. Effect of dissolved organic matter on the stability of magnetite nanoparticles under different pH and ionic strength conditions. Sci. Total Environ. 408 (16), 3477–3489.
Huynh, K.A., McCaffery, J.M., Chen, K.L., 2012. Heteroaggregation of multiwalled carbon nanotubes and hematite nanoparticles: rates and mechanisms. Environ. Sci. Technol. 46 (11), 5912–5920.
Kaegi, R., Voegelin, A., Ort, C., Sinnet, B., Thalmann, B., Krismer, J., Hagendorfer, H., Elumelu, M., Mueller, E., 2013. Fate and transformation of silver nanoparticles in urban wastewater systems. Water Res. 47 (12), 3866–3877.
Keller, A., McFerran, S., Lazareva, A., Suh, S., 2013. Global life cycle releases of engineered nanomaterials. J. Nanoparticle Res. 15 (6), 1–17.
Keller, A.A., Lazareva, A., 2013. Predicted releases of engineered nanomaterials: from global to regional to local. Environ. Sci. Technol. Lett. 1 (1), 65–70.
Keller, A.A., Wang, H.T., Zhou, D.X., Lenihan, H.S., Cherr, G., Cardinale, B.J., Miller, R., Ji, Z.X., 2010. Stability and aggregation of metal oxide nanoparticles in natural aqueous matrices. Environ. Sci. Technol. 44 (6), 1962–1967.
Labille, J., Harns, C., Bottero, J.-Y., Brant, J.A., 2015. Heteroaggregation of titanium dioxide nanoparticles with natural clay colloids. Environ. Sci. Technol. http://dx.doi.org/10.1021/acs.est.5b00357.
Lazareva, A., Keller, A.A., 2014. Estimating potential life cycle releases of engineered nanomaterials from wastewater treatment plants. ACS Sustain. Chem. Eng. 2 (7), 1656–1665.
Liang, Y., Bradford, S.A., Simunek, J., Heggen, M., Vereecken, H., Klumpp, E., 2013. Retention and remobilization of stabilized silver nanoparticles in an undisturbed loamy sand soil. Environ. Sci. Technol. 47 (21), 12229–12237.
Ma, H.-Z., Wang, B., 2006. Multifunctional microsized modified kaolin and its application in wastewater treatment. J. Hazard. Mater. 136 (2), 365–370.
Ma, H., Wang, B., Wang, Y., 2007. Application of molybdenum and phosphate modified kaolin in electrochemical treatment of paper mill wastewater. J. Hazard. Mater. 145 (3), 417–423.
McBride, M.B., 1994. Environmental chemistry of soils. Oxford university press.
Mohd Omar, F., Abdul Aziz, H., Stoll, S., 2014. Aggregation and disaggregation of ZnO nanoparticles: influence of pH and adsorption of Suwannee river humic acid. Sci. Total Environ. 468, 195–201.
Nandi, B.K., Goswami, A., Purkait, M.K., 2009. Adsorption characteristics of brilliant green dye on kaolin. J. Hazard. Mater. 161 (1), 387–395.
Olmedo, D.G., Tasat, D.R., Guglielmotti, M.B., Cabrini, R.L., 2005. Effect of titanium dioxide on the oxidative metabolism of alveolar macrophages: an experimental study in rats. J. of Biomed. Mater. Res. Part A 73A (2), 142–149.
Praetorius, A., Labille, J., Scheringer, M., Thill, A., Hungerbühler, K., Bottero, J.-Y., 2014. Heteroaggregation of titanium dioxide nanoparticles with model natural colloids under environmentally relevant conditions. Environ. Sci. Technol. 48 (18), 10690–10698.
Qi, J., Ye, Y.Y., Wu, J.J., Wang, H.T., Li, F.T., 2013. Dispersion and stability of titanium dioxide nanoparticles in aqueous suspension: effects of ultrasonication and concentration. Water Sci. Technol. 67 (1), 147–151.
Ross, C.S., Kerr, P.F., 1930. THE kaolin minerals1. J. Am. Ceram. Soc. 13 (3), 151–160.
Solomon, D.H., Hawthorne, D.G., 1983. Chemistry of Pigments and Fillers. Wiley.
Song, U., Jun, H., Waldman, B., Roh, J., Kim, Y., Yi, J., Lee, E.J., 2013. Functional analyses of nanoparticle toxicity: a comparative study of the effects of TiO_2 and Ag on tomatoes (Lycopersicon esculentum). Ecotoxicol. And Environ. Saf. 93, 60–67.
Theron, J., Walker, J.A., Cloete, T.E., 2008. Nanotechnology and water treatment: applications and emerging opportunities. Crit. Rev. Microbiol. 34 (1), 43–69.
Thio, B.J.R., Montes, M.O., Mahmoud, M.A., Lee, D.-W., Zhou, D., Keller, A.A., 2012. Mobility of capped silver nanoparticles under environmentally relevant conditions. Environ. Sci. Technol. 46 (13), 6985–6991.
Tombacz, E., Szekeres, M., 2004. Colloidal behavior of aqueous montmorillonite suspensions: the specific role of pH in the presence of indifferent electrolytes. Appl. Clay Sci. 27 (1–2), 75–94.
Tombacz, E., Szekeres, M., 2006. Surface charge heterogeneity of kaolinite in aqueous suspension in comparison with montmorillonite. Appl. Clay Sci. 34 (1–4), 105–124.
Trouiller, B., Reliene, R., Westbrook, A., Solaimani, P., Schiestl, R.H., 2009. Titanium dioxide nanoparticles induce DNA damage and genetic instability in vivo in mice. Cancer Res. 69 (22), 8784–8789.
Van Olphen, H., 1963. Introduction to Clay Colloid Chemistry.
Van Olphen, H., Fripiat, J., 1979. Data Handbook for Clay Minerals and Other Nonmetallic Materials. Pergamon, New York.
Wan, J.M., Tokunaga, T.K., 2002. Partitioning of clay colloids at air-water interfaces. J. colloid interface Sci. 247 (1), 54–61.
Wang, H., Qi, J., Keller, A.A., Zhu, M., Li, F., 2014. Effects of pH, ionic strength and humic acid on the removal of TiO_2 nanoparticles from aqueous phase by coagulation. Colloids Surfaces A: Physicochem. Eng. Aspects 450 (0), 161–165.
Wang, H.T., Keller, A.A., Clark, K.K., 2011. Natural organic matter removal by adsorption onto magnetic permanently confined micelle arrays. J. Hazard. Mater. 194, 156–161.
Wang, H.T., Keller, A.A., Li, F.T., 2010. Natural organic matter removal by adsorption onto carbonaceous nanoparticles and coagulation. J. Environ. Engineering-Asce 136 (10), 1075–1081.
Wang, H.T., Ye, Y.Y., Qi, J., Li, F.T., Tang, Y.L., 2013. Removal of titanium dioxide nanoparticles by coagulation: effects of coagulants, typical ions, alkalinity and natural organic matters. Water Sci. And Technol. 68 (5), 1137–1143.
Westerhoff, P., Song, G.X., Hristovski, K., Kiser, M.A., 2011. Occurrence and removal of titanium at full scale wastewater treatment plants: implications for TiO_2 nanomaterials. J. Environ. Monit. 13 (5), 1195–1203.
Zhang, X.Z., Sun, H.W., Zhang, Z.Y., Niu, Q., Chen, Y.S., Crittenden, J.C., 2007. Enhanced bioaccumulation of cadmium in carp in the presence of titanium dioxide nanoparticles. Chemosphere 67 (1), 160–166.
Zhao, J., Liu, F., Wang, Z., Cao, X., Xing, B., 2015. Heteroaggregation of graphene oxide with minerals in aqueous phase. Environ. Sci. Technol. 49 (5), 2849–2857.
Zheng, Z., He, P.J., Zhang, H., Shao, L.M., 2008. Role of dissolved humic substances surrogates on phthalate esters migration from sewage sludge. Water Sci. Technol. 57 (4), 607–612.
Zhou, D.X., Abdel-Fattah, A.I., Keller, A.A., 2012. Clay particles destabilize engineered nanoparticles in aqueous environments. Environ. Sci. Technol. 46 (14), 7520–7526.
Zhu, M., Wang, H., Keller, A.A., Wang, T., Li, F., 2014. The effect of humic acid on the aggregation of titanium dioxide nanoparticles under different pH and ionic strengths. Sci. Total Environ. 487 (0), 375–380.